Int j simul model 22 (2023) 4, 643-654
Original scientific paper

SIMULATION METHOD FOR STITCH WIRE VIBRATION LOAD AND FATIGUE LIFE

Liu, J. D.; Chen, J. Q.; Wu, J. Q.; Han, F. & Guan, J. F.[#]
School of Electrical Engineering, Southwest Jiaotong University, Chengdu 611756, China
E-Mail: kwanjinfa@163.com ([#] Corresponding author)

Abstract
Stitch wire is the key component in high-speed railway catenary. During the construction and operation of the catenary, tension changes can lead to fracture of the stitch wire. This study proposed a simulation method considering the structure and stress distribution of stitch wire to reveal the effect of tension changes on the fatigue life. Dynamic simulation model at a speed of 300 km/h was constructed to obtain the vibration load. A refined model of stitch wire was used to simulate the contact between the structures. Finally, the fatigue life of stitch wire was calculated when the tension changes by analysing the stress distribution under vibration. Results demonstrate that the lifting effect of the pantograph during operation causes vertical vibrations of stitch wire, and the stress concentration position is located at the connection with its clamp. As the tension increases form 2.0 kN to 5.0 kN, the range of vibration angle at the clamp decreases from 2.73° to 1.33°, and fatigue life increases from 1.36×10^6 to 8.76×10^6. The proposed method provides an accurate approach to simulate the load and fatigue life of stitch wire under real working conditions.
(Received in June 2023, accepted in October 2023. This paper was with the authors 6 weeks for 2 revisions.)

Key Words: High-Speed Railway, Stitch Wire, Vibration, Fatigue Life, Simulation Model

1. INTRODUCTION

The catenary of Chinese high-speed railway adopts elastic suspension, which mainly consists of contact wire, messenger wire, dropper, and stitch wire [1]. The stitch wire is fixed on the messenger wire, and the contact wire is suspended from the stitch wire dropper. Given its uneven elasticity, the catenary undergoes coupled vibration when the pantograph passes at high speed, causing the catenary components to bear moving and impact loads [2]. The significant changes in the internal stress of the catenary components lead to fatigue fracture [3]. During maintenance of the Wuhan–Guangzhou high-speed railway catenary, the stitch wire was found to had broken at the clamp. Investigation reveals that the tension distribution of stitch wire is within the range of 2.0–5.0 kN, which does not maintain the design requirement of 3.5±0.35 kN. Tension changes in the stitch wire may be the key factor causing fatigue fracture. The load of stitch wire under different tensions cannot be obtained through on-site measurement because of the special working environment and the requirements for operational safety of high-speed railway.

Previous studies on the vibration load and fatigue life of stitch wire remain limited. In terms of fatigue research on catenary components, scholars focused on issues such as contact line friction and wear, contact line fatigue, dropper fatigue and support device fatigue. Few studies analysed the stress distribution of the stranded wire structure of catenary components, and the influence of the stranded wire structure on fatigue is ignored. The dropper and stitch wire are both stranded structures, the fatigue research on the dropper shows that the dropper is prone to fatigue fracture at the clamp position under alternating stress loads [4]. However, studies on the dropper under impact loads cannot be used for vibration and fatigue analysis of stitch wire. To ensure the safe operation of high-speed railway, the stress changes and fatigue life of stitch wire during service should be studied. Thus, the simulation method for analysing the stress distribution and calculating the fatigue life of stitch wire needs to be established.

Based on the abovementioned analysis, this study uses finite element simulation and fatigue life calculation to analyse the vibration load and fatigue life of stitch wire, and clarifies the influence of tension changes.

2. STATE OF THE ART

The operating conditions must be determined when studying the fatigue life of railway mechanical equipment. The fatigue analysis and optimization of railway vehicles were carried out by processing and synthesizing vibration data into load spectra that can reflect environmental vibration characteristics, demonstrating the importance of real vibration loads in fatigue research [5]. Sampayo et al. [6] proposed a system design method that combines multi body simulation and finite element analysis to evaluate the stress state of go-kart during operation and achieve optimal vehicle design. Kraft and Lüdicke [7] obtained equipment operating loads through multi body simulation, analysed the impact of operating conditions and loads on damage using sensitivity analysis, and estimated equipment damage using a finite element model. Few studies focused on the vibration load and fatigue life of stitch wire, for which tension is an important parameter. Li et al. [8] studied the effect of stitch wire tension on the dynamic performance of the pantograph–catenary by using a dynamic interaction simulation model. The dynamic performance improved when the tension increased from 2.8 kN to 3.8 kN, but the vibration loads of stitch wire during such changes have not been studied. Qi et al. [9] constructed a pantograph–catenary system with different speeds in the finite element software ANSYS and compiled load spectra for components such as contact and messenger wires, but did not include stitch wire. The alternating load of components can be obtained through finite element software to calculate their fatigue life [10]. Li et al. [11] built an integrated platform that can achieve the construction of a pantograph–catenary system with vibration and fatigue life analysis. However, the catenary wires are equivalent to rod or beam elements, and the stress distribution of the structure cannot be obtained. Chen et al. [12] equated the dropper vibration to the harmonic forced vibration of the catenary, and studied the effects of excitation frequency and amplitude on the fatigue life of dropper as a whole. The contact wire must be equivalent to the beam element to simulate the stress change and estimate the fatigue life based on the material performance curve obtained from the experiment [13]. Thomas et al. [14] studied the effects of clamp radius and bolt torque on bending fretting fatigue of overhead conductors, but neglected the changes in vibration amplitude under actual working loads. Yang et al. [15] established 8 types of finite element models for ring welded joints and proposed a fatigue assessment method for predicting the fatigue life of unknown plate thick ring welded joints based on the *S*-*N* curve. The simulation method for obtaining component loads through finite element models and calculating fatigue life was combined. Said et al. [16] simulated the fretting wear of overhead transmission lines through fatigue tests and analysed the contact stress between strands using a finite element model. Omrani et al. [17, 18] studied the inter-wire wear of overhead aluminium stranded wires at the clamp through single line tests, and found that vibration displacement is the main influencing factor. Simulation and tests on the fatigue of steel wire ropes indicate that the bending load and tension affect the internal stress distribution and wear [19]. Chen et al. [20] constructed a refined model of a steel wire rope with internal defects to analyse the fatigue life under bending load, but this refined simulation method has not been applied to the stress analysis of stitch wire.

The abovementioned studies mainly focused on the simulation of vibration loads and fatigue life prediction of the dropper, steel wire ropes, and overhead transmission lines. No analysis has been conducted on the vibration load changes of stitch wire during service, and there is a lack of research on stress distribution and fatigue life prediction. Therefore, this study

proposes a simulation method that can obtain the vibration load, stress distribution, and fatigue life of stitch wire in the working environment.

The remainder of this study is organized as follows. Section 3 elaborates on the methods used to obtain the vibration load and the refined model that can calculate the stress distribution of stitch wire. A simulation framework for calculating the fatigue life is constructed, and the damage accumulation method is introduced. Section 4 discusses the load spectrum of stitch wire under the specified working environment, presents the analysis on stress distribution under vibration load, and calculates the fatigue life. Section 5 summarizes the conclusions drawn from this study.

3. METHODOLOGY

3.1 Dynamic simulation model of the pantograph–catenary

The vibration load of stitch wire under service can be extracted by using the dynamic simulation model of the pantograph–catenary. With the Wuhan–Guangzhou high-speed railway as an example, this study adopts a direct modelling method to establish a pantograph–catenary simulation model [21]. The design parameters are listed in Table I. The cable, beam, and lumped mass elements are selected to construct its catenary model, and the dynamic equation of the catenary can be assembled as:

$$M_j\ddot{u}_j + C_j\dot{u}_j + K_j u_j + K_{ct}u_j + K_x u_j = G_j + F_{cf} + F_{Tf} \tag{1}$$

In the formula, M_j is the mass matrix, u_j is the node displacement matrix, C_j is the Rayleigh damping matrix, K_j is the elastic stiffness matrix, K_{ct} is the geometric stiffness matrix, K_x is the suspension string Elastic stiffness matrix, G_j is the gravity matrix, F_{cf} is the dynamic contact force matrix of the pantograph, and F_{Tf} is the tension matrix of the catenary.

Table I: Design parameters of the Wuhan–Guangzhou high-speed railway catenary.

Variable	Unit	Value
Span	m	50
Mass per unit of messenger wire	kg/m	1.08
Mass per unit of contact wire	kg/m	1.35
Tension of messenger wire	kN	21.0
Tension of contact wire	kN	30.0
Length of stitch wire	m	14
Tension of stitch wire	kN	3.5

The equivalent model parameters of pantograph DSA380 [22] are listed in Table II. The differential equation of the pantograph is:

$$\begin{cases} m_1\ddot{y}_1 + (c_1 + c_2)\dot{y}_1 + (k_1 + k_2)y_1 - c_2\dot{y}_1 - k_2 y_1 = f_0 \\ m_2\ddot{y}_2 + (c_3 + c_2)\dot{y}_2 + (k_3 + k_2)y_2 - c_3\dot{y}_3 - k_3 y_3 - c_1\dot{y}_1 - k_1 y_1 = 0 \\ m_3\ddot{y}_3 + c_3\dot{y}_3 + k_3 y_3 - c_3\dot{y}_2 - k_3 y_2 = -F_j \end{cases} \tag{2}$$

In the formula, m_1, m_2, m_3 are the equivalent masses of the lower arm, upper frame, and bow head, y_1, y_2, y_3 represent the vertical displacements of the lower arm, upper frame, and bow head, c_1, c_2, c_3 are the equivalent damping values of the lower arm, upper frame, and bow head, k_1, k_2, k_3 are the equivalent damping equivalent stiffness of the lower arm, upper frame, and bow head, f_0 is the static lifting force of the pantograph, and F_j is the dynamic contact force between the pantograph and catenary.

Subsequently, the penalty function method is used to construct a virtual spring between contact pairs to calculate the contact force. In a contact pair, when the surfaces are not in touch, the spring is in a failure state. Only when the surfaces of the contact pair are in touch with each other and an intrusion distance is generated, the spring is compressed and the contact force be generated.

Table II: Equivalent model parameters of pantograph.

Variable	Unit	Value
m_1	kg	5.8
m_2	kg	6.0
m_3	kg	7.12
c_1	Ns/m	70
c_2	Ns/m	0
c_3	Ns/m	0
k_1	N/m	0.1
k_2	N/m	14100
k_3	N/m	9430

The catenary model is exhibited in Fig. 1. The labels 1–10 represent the stitch wire selected in the analysis section, with 1–5 in the first anchor section, 6–10 in the second anchor section, and 4–7 are within the joint of the 5-span anchor segment. Through the dynamic simulation model, the vibration displacement and tension time history data of any position on the stitch wire can be calculated.

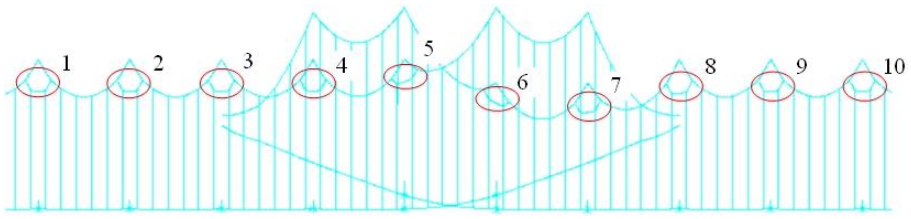

Figure 1: Simulation model of catenary.

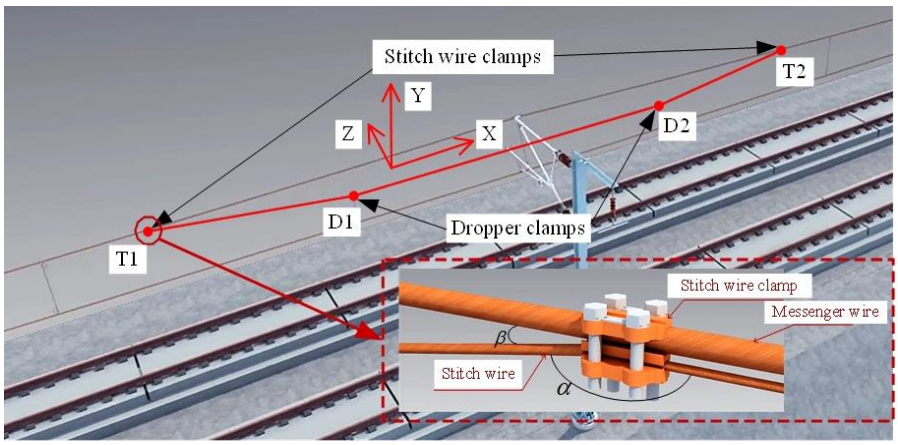

Figure 2: Schematic diagram for service analysis of stitch wire.

In Fig. 2, the stitch wire is connected to the contact suspension through stitch wire clamps T1/T2 connected to the messenger wire and dropper clamps D1/D2 connected to the contact wire. The stitch wire clamps T1/T2 provide tension, and the dropper clamps D1/D2 transmit the gravity of the contact wire. In this study, we define the direction along the line as the X direction, the vertical upward direction perpendicular to the ground as the Y direction, and the

vertical direction perpendicular to the line as the Z direction, α is the bending angle of the stitch wire during vibration, and β is the angle between the stitch wire and the messenger wire.

When the pantograph passes, the load on stitch wire is reduced and deformed due to the lifting effect on the contact suspension. At this time, the stitch wire is in a relatively unloaded state. When the pantograph has passed, the contact suspension falls back and generates an impact load that causes continuous vibration of stitch wire. Such vibration is mainly manifested in the Y direction, and the variations of their vibration load are represented by the bending angle. The smaller the value, the greater the degree of wire bending.

3.2 Refined model of stitch wire

The refined model reflects the specific composition of the structure and can accurately analyse the local stress of stitch wire. In this study, the stitch wire was made of JTMH35 copper alloy stranded wire and using 1×7 strand structure, with an outer diameter of 7.50 mm and a single wire diameter of 2.50 mm. The strength and life of the wire depend on the material properties and stress distribution. The material properties of stitch wire are listed in Table III. A three-dimensional model of stitch wire clamp and cable strand was constructed in UG, as depicted in Fig. 3 a and 3 b. The stitch wire clamp was composed of upper clamp, middle clamp, lower clamp and connecting bolts.

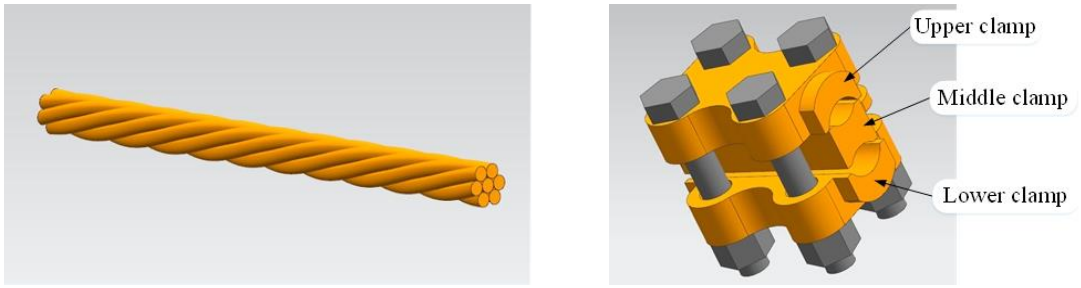

a) b)

Figure 3: Stitch wire and its clamp model: a) stitch wire, b) stitch wire clamp.

Table III: Material properties of stitch wire.

Variable	Unit	Value
Young's modulus	GPa	113
Tensile strength	MPa	620
Poisson's ratio	–	0.3

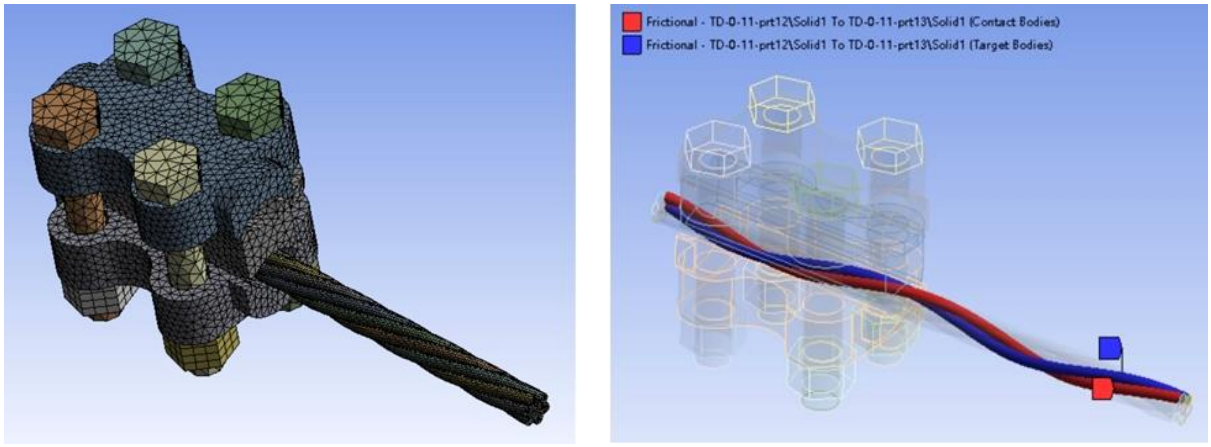

a) b)

Figure 4: Refined model of stitch wire: a) mesh, b) contact between wires.

In Fig. 4 a, the model is imported into the LS-DYNA module. Frictional contact is established on the surface of the stitch wire to simulate the interaction between wires, as illustrated in Fig. 4 b. Boundary conditions and load settings are carried out to obtain the stress distribution and stress changes of stitch wire under the specified load in the simulation.

3.3 Fatigue simulation of stitch wire

Fig. 5 shows the fatigue simulation framework diagram of the stitch wire. The stress changes of stitch wire under specified vibration state are evaluated in the LS-DYNA module. The stress data are imported into ANSYS nCode DesignLife, the material properties and fatigue calculation method are set, and the fatigue life under this vibration state is obtained.

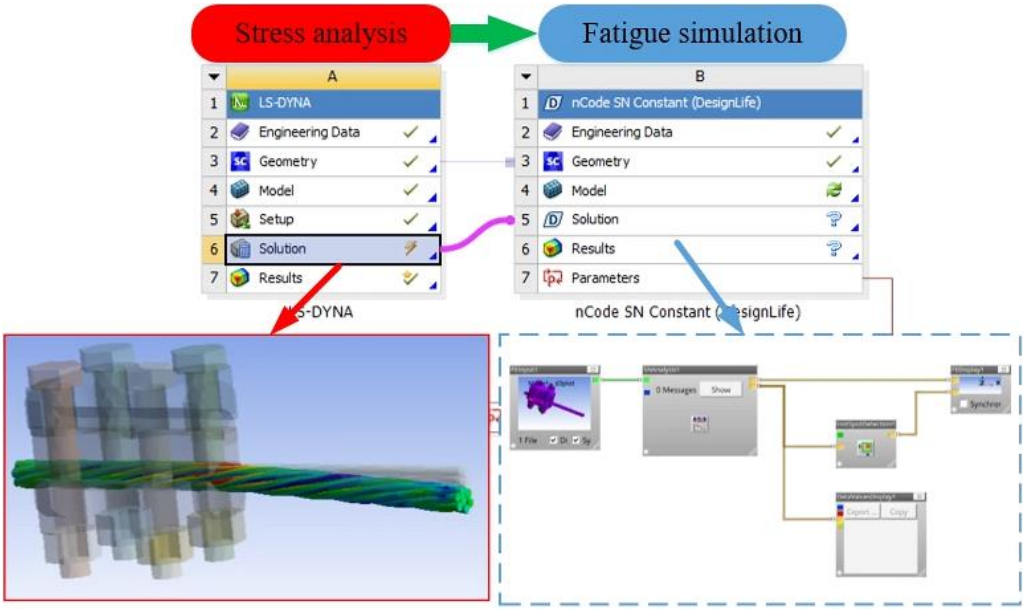

Figure 5: Fatigue simulation framework for stitch wire.

The load spectrum contains cyclic loads of different sizes when the pantograph passes through. In fatigue analysis, to comprehensively calculate the contribution of all loads to the fatigue is necessary. Linear fatigue cumulative damage theory suggests that under working conditions, structures continuously endure fatigue damage caused by alternating loads in a linear accumulation, and the stresses under each load are independent and uncorrelated with each other. Fatigue failure occurs when the cumulative load damage to the structure reaches the fatigue limit. The representative of linear fatigue cumulative damage theory is Miner fatigue damage theory, which based on the *S-N* curve of materials or structures. Defines fatigue life as N_i when the load is S_i and the number of loading times as n_i, the cumulative damage D of the structure under different load levels is:

$$D = \sum_{i=1}^{k} D_i = \sum_{i=1}^{k} \frac{n_i}{N_i} \tag{3}$$

The structure undergoes fatigue failure when the cumulative damage D reaches 1.

4. RESULT ANALYSIS AND DISCUSSION

4.1 Vibration load of stitch wire

The dynamic simulation model in section 3.1 was used to obtain the vibration load of stitch wire during operations, as illustrated in Fig. 6. During the vibration, the tension shows a small

fluctuation range, and the tension with the smallest vibration angle fluctuates around the static tension of 3.5 kN. From the static angle analysis, at the joint position of the anchor section, the elevation of the contact suspension upper and lower anchors and the change in structural height cause a change in the static angle of the stitch wire. The minimum vibration angle is 175.76 °, which occurs at position 4-T2 numbered 8. At this position, the variation curve of the vibration angle plotted in Fig. 7. After 15 seconds of the pantograph passing through, the vibration angle cycles back and forth between 176.25 °–177.00 °, a long-term on-site operation indicates that this cyclic load is within the fatigue limit. Therefore, simplify the vibration load with a threshold of 0.75 °, and the simplified vibration angle consists of 58 broken lines, forming 29 sets of cyclic loads.

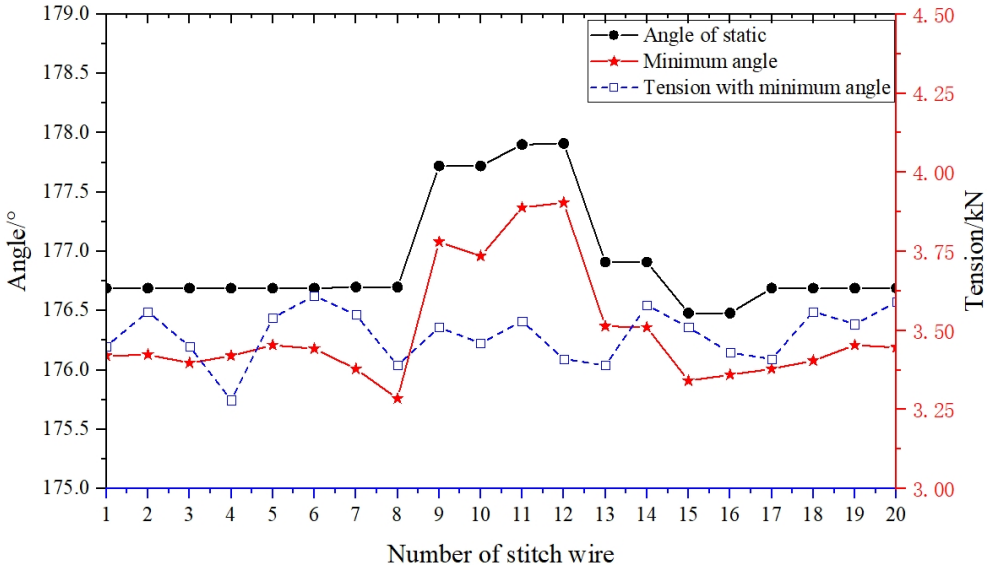

Figure 6: Statistical analysis of changes in tension and angle in the analysis section.

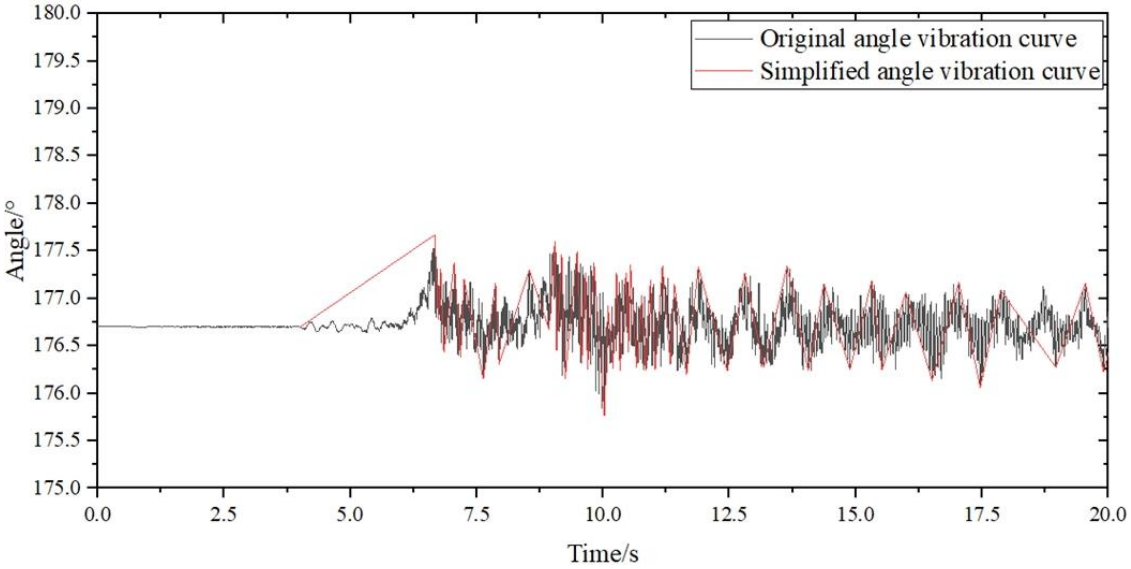

Figure 7: Comparison of original and simplified curves of vibration angle.

Table IV shows the vibration loads of stitch wire with tensions of 2.0, 3.5, and 5.0 kN. As the tension increases, the vibration bending gradually decreases. The increase in tension reduces the deformation of stitch wire under the same load. The maximum vibration range is 2.73° when the tension is 2.0 kN, the maximum vibration range is 1.91 ° when the tension is 3.5 kN, and the maximum vibration range is 1.33 ° when the tension is 5.0 kN.

Table IV: Vibration load statistics under different tensions.

Tension (kN)	**Angular range** (°)	**Static angle** (°)	**Minimum angle** (°)	**Maximum angle** (°)	**Number of cycles**
2.0	0.75–1.0	175.66	175.00	175.84	6
	1.0–2.0		174.83	176.14	23
	2.0–3.0		174.52	176.94	1
			174.39	177.12	1
3.5	0.75–1.0	176.69	176.37	177.17	17
	1.0–2.0		176.17	177.39	12
	Max		175.76	177.67	1
5.0	0.75–1.0	177.32	176.98	177.78	10
	1.0–2.0		176.75	177.85	8
	Max		176.59	177.92	1

4.2 Stress distribution of stitch wire

The refined model of stitch wire in section 3.2 was used to evaluate the stress distribution and changes under different vibration loads, as shown in Fig. 8. Set the tension to 3.5 kN and uses the angle change during the vibration as the input condition. The initial angle is 176.69 °, which is converted into a displacement of 4.33 mm at the end of the model. The maximum angle during bending is 175.76 °, and the bending from the starting position is from 1.22 mm to 5.55 mm. The minimum bending angle is 177.67 °, and moves 1.28 mm upward from the starting position to reach 3.05 mm. The analysis time is 0.07 s, the pre-tightening force of the clamp bolt is set at 0.001 s, and the end of stitch wire is bent to the static angle position at 0.005 s.

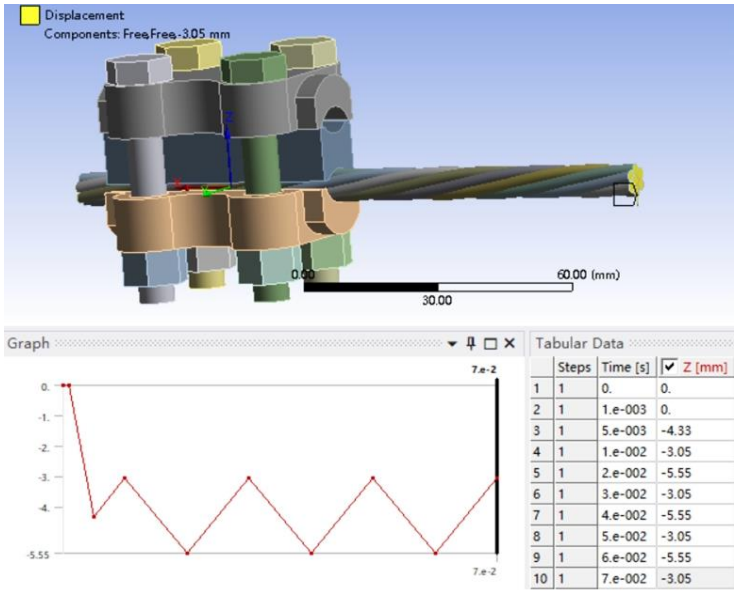

Figure 8: Vibration displacement of stitch wire.

Fig. 9 shows the stress distribution of each wire when the stitch wire reaches its maximum bending during the vibration. The three metal wires J_0, J_1, J_4 in the middle row shows greater stress, which reaches a maximum value of 281.71 MPa. J_0 is the core wire of stitch wire. The stress at the bending point increases when subjected to force bending.

The stress distribution obtained by simulation is set according to the maximum vibration loads when the tensions are set to 2.0 and 5.0 kN. The maximum stress loads reached 295.64 MPa when the tension is 2.0 kN and the vibration angle is 174.39 °, as shown in Fig. 10 a. In Fig. 10 b, the maximum stress loads reached 287.16 MPa when the tension is 5.0 kN and the vibration angle is 176.59 °.

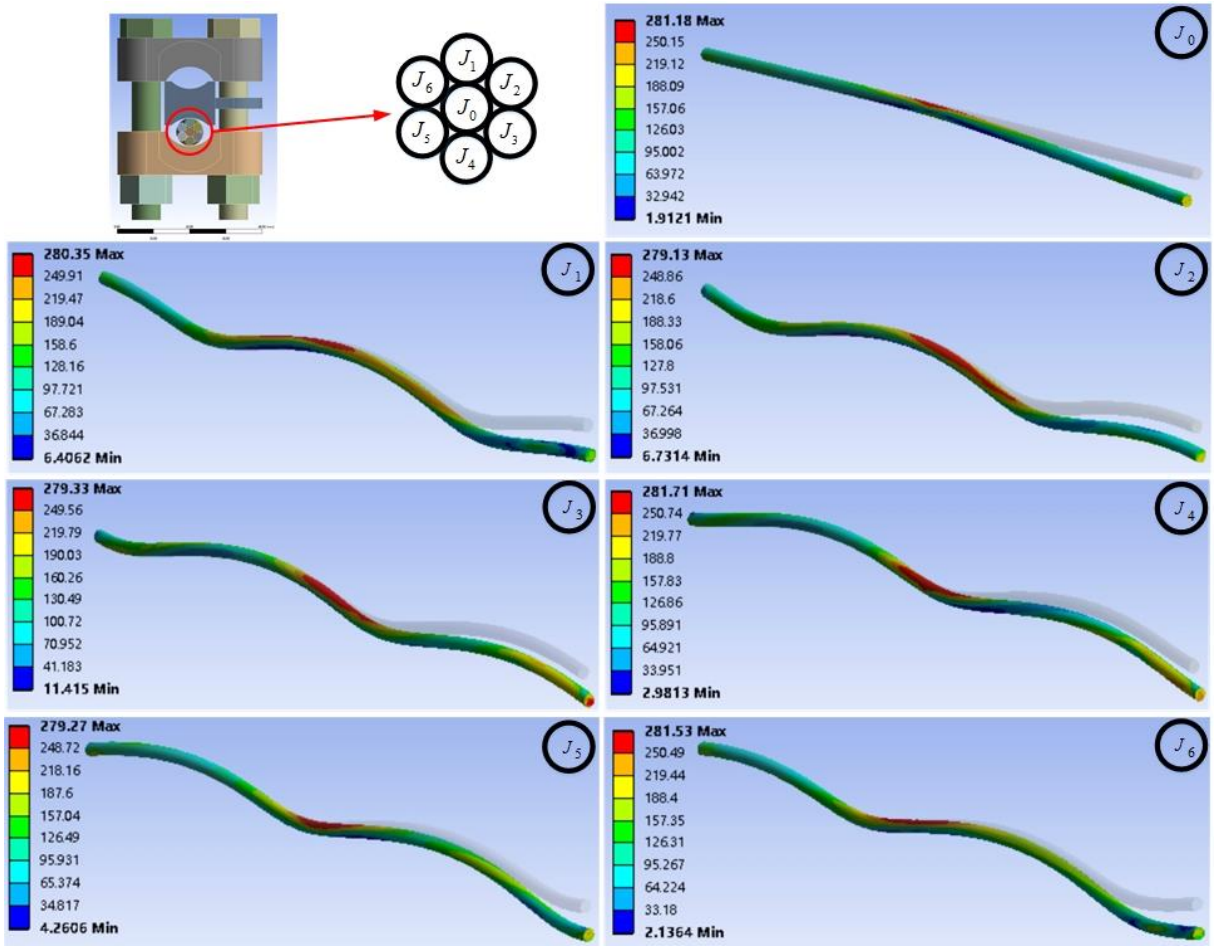

Figure 9: Stress distribution of stitch wire during maximum bending.

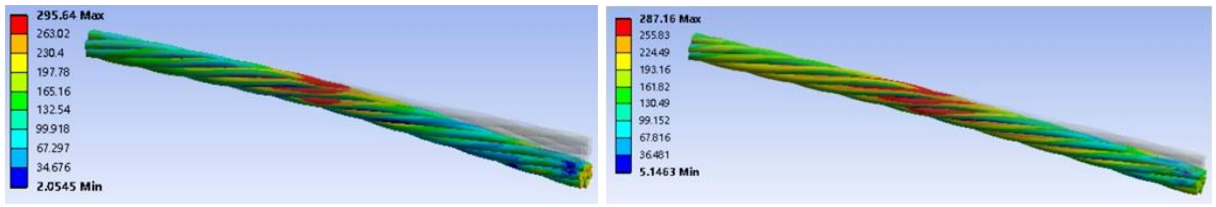

a) b)

Figure 10: Stress distribution of stitch wire at maximum bending after changes in tension: a) tension is 2.0 kN, b) tension is 5.0 kN.

4.3 Fatigue life of stitch wire

Fig. 11 reflects the simulation results of fatigue life under vibration loads using the fatigue simulation method in section 3.3. The fatigue life near the end of the stitch wire are excluded due to the influence of boundary effects in the simulation. For stitch wire with a tension of 3.5 kN, the minimum fatigue life occurs at the connection between the stitch wire and the clamp. The fatigue life under different vibration loads are listed in Table V.

Table V: Fatigue life of stitch wire under different vibrations.

Angular range (°)	**Minimum angle** (°)	**Maximum angle** (°)	**Fatigue life**	**Number of loads**
0.75–1.0	176.37	177.17	1.44×10^{9}	17
1.0–2.0	176.17	177.39	1.17×10^{8}	12
Max	175.76	177.67	8.88×10^{6}	1

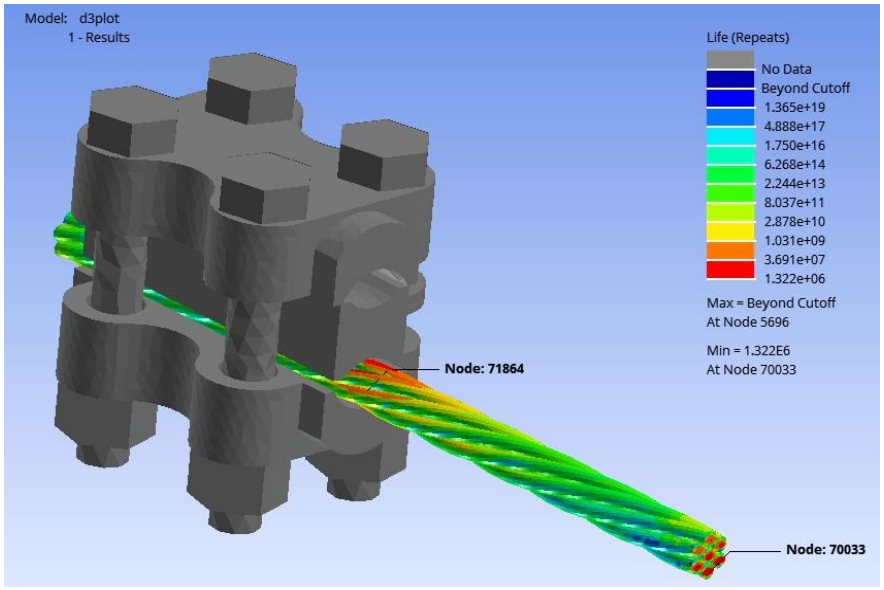

Figure 11: Fatigue simulation of stitch wire.

Using the Miner linear damage accumulation principle in section 3.3, the calculated fatigue life of stitch wire at a speed of 300 km/h is 4.58×10^6 arches. If 17 groups of loads with vibration angle ranges of 0.75 °–1.0 ° are omitted, then the fatigue life is 4.84×10^6 arches. These single cycle loads affect 0.31 % of the change in fatigue life, and thus vibration loads within this range are ignored in subsequent fatigue life calculations.

The fatigue life when the tension is 2.0 kN are listed in Table VI. The fatigue life is simulated under three different vibration loads, and the fatigue life of stitch wire is calculated to be 1.36×10^6 arches according to the principle of cumulative fatigue damage. The maximum vibration range increased by 42.9 % from 1.91 ° to 2.73 °, and the fatigue life decreased by 71.9 % from 4.84×10^6 to 1.36×10^6 after the pantograph passes.

Table VI: Fatigue life of stitch wire with a tension of 2.0 kN.

Angular range (°)	**Minimum angle** (°)	**Maximum angle** (°)	**Fatigue life**	**Number of loads**
1.0–2.0	174.83	176.14	1.80×10^8	23
2.0–3.0	174.52	176.94	4.99×10^6	1
	174.39	177.12	2.45×10^6	1

The fatigue life when the tension is 5.0 kN are listed in Table VII. The fatigue life under two different vibration loads is simulated and calculated as 8.76×10^6 arches. The maximum vibration range decreased by 30.4 % from 1.91 ° to 1.33 °, and fatigue life increased by 80.9 % from 4.84×10^6 to 8.76×10^6.

Table VII: Fatigue life of stitch wire with a tension of 5.0 kN.

Angular range (°)	**Minimum angle** (°)	**Maximum angle** (°)	**Fatigue life**	**Number of loads**
1.0–2.0	176.75	177.85	7.78×10^7	8
Max	176.59	177.92	4.14×10^7	1

5. CONCLUSION

A dynamic simulation model of the pantograph–catenary and refined and fatigue simulation models of the stitch wire were constructed. The vibration load, stress distribution, and fatigue

life were analysed and compared when tension changes. Taking the design parameters of the Wuhan–Guangzhou high-speed railway as an example, this study was carried out at a speed of 300 km/h. The following conclusions can be drawn:

(1) When the pantograph passes at high speed, the vibration caused by the lifting effect of the contact suspension causes the stitch wire to continuously bend at the clamp and experience fatigue fracture. As the tension increases, the stitch wire thread tightens and the vibration at the clamp decreases.

(2) The maximum stress concentration of stitch wire during the vibration is distributed at its connection with the clamp. When the tension remains constant, the smaller the vibration angle, the greater the stress load.

(3) As the tension of stitch wire increases, the fluctuation range of the vibration angle decreases, alternating stress decreases, and the fatigue life gradually increases.

Thus, this study proposes a method of finite element simulation and fatigue calculation to analyse the effect of tension changes on the vibration load and fatigue life of stitch wire. The proposed method provides theoretical support for the need of further research on the fatigue fracture problem in engineering. However, given the lack of *S-N* curve, the ultimate tensile strength is used for estimation in fatigue life calculation. The fatigue simulation model is modified based on the fatigue test to improve the accuracy of fatigue life calculation of stitch wire.

ACKNOWLEDGEMENT

This work was supported by the China National Railway Group Limited (Q110420S04009).

REFERENCES

[1] Wu, J. (2018). *Pantograph and Contact Line System*, 1st edition, Academic Press, London, doi:10.1016/C2016-0-02570-6

[2] Qi, G.; Zhao, H.; Xiao, X.; Xu, H.; Li, H. (2018). Numerical simulation of dynamic stress and analysis of fatigue load characteristics for high-speed railway catenary droppers, *China Mechanical Engineering*, Vol. 29, No. 9, 1063-1068, doi:10.3969/j.issn.1004-132X.2018.09.009

[3] Chen, L. (2018). Study on dynamic force of integral dropper of catenary under action of high-speed pantograph, *China Railway Science*, Vol. 39, No. 3, 86-92, doi:10.3969/j.issn.1001-4632.2018.03.12

[4] Qin, Y.; Xiao, S.; Lu, L.; Yang, B.; Zhu, T.; Yang, G. (2022). Fatigue failure of integral droppers of high-speed railway catenary under impact load, *Engineering Failure Analysis*, Vol. 134, Paper 106086, 17 pages, doi:10.1016/j.engfailanal.2022.106086

[5] You, T.; Zhou, J.; Gong, D.; Sun, Y.; Li, B.; Chen, J. (2022). Synthesis of random vibration environment spectra for the fatigue analysis and optimization of railway vehicles, *International Journal of Fatigue*, Vol. 159, Paper 106752, 16 pages, doi:10.1016/j.ijfatigue.2022.106752

[6] Sampayo, D.; Luque, P.; Mantaras, D. A.; Rodriguez, E. (2021). Go-kart chassis design using finite element analysis and multibody dynamic simulation, *International Journal of Simulation Modelling*, Vol. 20, No. 2, 267-278, doi:10.2507/IJSIMM20-2-555

[7] Kraft, S.; Lüdicke, D. (2022). Sensitivity analysis for operating loads in fatigue design of railway vehicles, *Proceedings of the Institution of Mechanical Engineers, Part F: Journal of Rail and Rapid Transit*, Vol. 236, No. 7, 826-837, doi:10.1177/09544097211045478

[8] Li, W.; Cui, X.; Chen, W.; Richmann, T. (2009). Research on the selection of parameters for the overhead contact line system with stitch wire on high-speed railway, *Journal of Railway Engineering Society*, Vol. 2009, No. 8, 82-87, doi:10.3969/j.issn.1006-2106.2009.08.020

[9] Qi, G.; Chen, J.; Xiao, X.; Song, Y. (2015). Fatigue load spectrum of key parts of high-speed railway catenary, *Journal of Railways*, Vol. 2015, No. 10, 48-53, doi:10.3969/j.issn.1001-8360.2015.10.007

[10] Yanez Rodriguez, J.; Yanez Contreras, P.; Santander Bastida, F. J.; Rodriguez, M. L.; Medina Flores, J. M.; Poblano Salas, C. A.; Barceinas Sanchez, J. D. O. (2022). Fatigue analysis of a rack tool to increase milling productivity, *DYNA*, Vol. 97, No. 4, 380-385, doi:10.6036/10425
[11] Li, F.; Luo, M.; Gao, J.; Huan, R. (2020). Analysis of three-dimensional catenary vibration and component fatigue life based on flexible multibody dynamics, *Electric Railway*, Vol. 2020, No. S1, 21-25, doi:10.19587/j.cnki.1007-936x.2020z1.003
[12] Chen, L.; Peng, P.; He, F. (2018). Fatigue life analysis of dropper used in pantograph-catenary system of high-speed railway, *Advances in Mechanical Engineering*, Vol. 10, No. 5, 10 pages, doi:10.1177/1687814018776135
[13] Xu, Z.; Song, Y.; Liu, Z. (2022). Stress analysis and fatigue life prediction of contact wire located at steady arms in high-speed railway catenary system, *IEEE Transactions on Instrumentation and Measurement*, Vol. 71, Paper 9001212, 12 pages, doi:10.1109/TIM.2022.3144747
[14] Thomas, O. O.; Chouinard, L.; Langlois, S. (2022). Probabilistic fatigue fragility curves for overhead transmission line conductor-clamp assemblies, *Frontiers in Built Environment*, Vol. 8, Paper 833167, 21 pages, doi:10.3389/fbuil.2022.833167
[15] Yang, L.; Yang, B.; Yang, G. W.; Xiao, S. N.; Zhu, T.; Wang, F. (2022). Fatigue-life evaluation method for ring-welded joints, *International Journal of Simulation Modelling*, Vol. 21, No. 2, 320-331, doi:10.2507/IJSIMM21-2-CO6
[16] Said, J.; Garcin, S.; Fouvry, S.; Cailletaud, G.; Yang, C.; Hafid, F. (2020). A multi-scale strategy to predict fretting-fatigue endurance of overhead conductors, *Tribology International*, Vol. 143, Paper 106053, 13 pages, doi:10.1016/j.triboint.2019.106053
[17] Omrani, A.; Langlois, S.; van Dyke, P.; Lalonde, S.; Karganroudi, S. S.; Dieng, L. (2021). Fretting fatigue life assessment of overhead conductors using a clamp/conductor numerical model and biaxial fretting fatigue tests on individual wires, *Fatigue & Fracture of Engineering Materials & Structures*, Vol. 44, No. 6, 1498-1514, doi:10.1111/ffe.13444
[18] Omrani, A.; Dieng, L.; Langlois, S.; van Dyke, P. (2022). Friction properties at the contact interfaces of overhead line aluminium conductors, *IEEE Transactions on Power Delivery*, Vol. 37, No. 1, 442-448, doi:10.1109/TPWRD.2021.3062704
[19] Peng, Y.; Huang, K.; Ma, C.; Zhu, Z.; Chang, X.; Lu, H.; Zhang, Q.; Xu, C. (2023). Friction and wear of multiple steel wires in a wire rope, *Friction*, Vol. 11, No. 5, 763-784, doi:10.1007/s40544-022-0665-y
[20] Chen, Y.; Chen, J.; Zhang, Y.; He, Y.; Xu, J.; Xiang, J. (2022). Effect of internal defect on the low-cycle bending fatigue behavior of a single-strand wire rope, *Construction and Building Materials*, Vol. 350, Paper 128874, 12 pages, doi:10.1016/j.conbuildmat.2022.128874
[21] Wu, M.; Xu, X.; Yan, Y.; Luo, Y.; Huang, S.; Wang, J. (2022). Multi-parameter joint optimization for double-strip high-speed pantographs to improve pantograph-catenary interaction quality, *Acta Mechanica Sinica*, Vol. 38, No. 1, Paper 521344, 11 pages, doi:10.1007/s10409-021-09018-x
[22] Guan, J.; Tian, Z.; Zhang, X. (2019). Influence of parameters of catenary stitch wire on dynamic performance between pantograph and catenary, *Journal of Southwest Jiaotong University*, Vol. 56, No. 3, 659-665, doi:10.3969/j.issn.0258-2724.20190326